

QUANTUM STATES AND LINEAR RESPONSE IN dc AND ELECTROMAGNETIC FIELDS FOR THE CHARGE CURRENT AND SPIN POLARIZATION OF ELECTRONS AT THE Bi/Si INTERFACE WITH THE GIANT SPIN–ORBIT COUPLING

*D. V. Khomitsky**

*Lobachevskii State University of Nizhny Novgorod
603950, Nizhny Novgorod, Russia*

Received July 15, 2011

An expansion of the nearly free-electron model constructed by Frantzeskakis, Pons, and Gioni [1] describing quantum states at the Bi/Si(111) interface with the giant spin–orbit coupling is developed and applied for the band structure and spin polarization calculation, as well as for the linear response analysis of the charge current and induced spin caused by a dc field and by electromagnetic radiation. It is found that the large spin–orbit coupling in this system may allow resolving the spin-dependent properties even at room temperature and at a realistic collision rate. The geometry of the atomic lattice combined with spin–orbit coupling leads to an anisotropic response for both the current and spin components related to the orientation of the external field. The in-plane dc electric field produces only the in-plane components of spin in the sample, while both the in-plane and out-of-plane spin components can be excited by normally propagating electromagnetic wave with different polarizations.

1. INTRODUCTION

The knowledge of materials with high values of spin-orbit (SO) coupling parameters is the goal of many theoretical, experimental, and device research groups in condensed matter physics and spintronics due to their fascinating spin-related properties and possible applications in the information processing and storage. Among the candidates that attract considerable attention in the last decade are Bi/Si(111) surface alloys whose band structure was experimentally studied for several years and recently modeled [1]. This material, in line with other examples of “metal-on-semiconductor” systems with large SO coupling, has been the subject of many experimental and theoretical papers because it seems very promising to use a material combining the large SO splitting of Bi and the conventional semiconductor technology of Si, which is one of the main goals of spintronics [2–4]. Here, we mention only some of the numerous results of research on the properties of a Bi-covered Si surface with various crystal orientations of the Si substrate. In par-

ticular, the scanning tunneling microscopy has been used to determine the surface structure of Bi/Si some 18 years ago [5], and the analysis of the atomic geometry and electronic structure continued in [6, 7], focusing mainly on the atomic surface geometry and spin-resolved band structure reconstruction, where the methods of angle-resolved photoemission spectroscopy have been applied [1, 8–15]. Other methods include the low-energy electron diffraction and atomic force microscopy [16, 17]. Besides pure Si, the Si–Ge superlattices have been used as a substrate for Bi coverage [18], and the lateral Ge–Si nanostructure prepared on the Si/Bi surface have been studied by scanning tunneling microscopy [19]. Also, for the Bi/Si system, there were studies of energetic stability and equilibrium geometry [20] and the possibility of designing iron silicide wires along Bi nanolines on the hydrogenated Si surface [21], and of the thermal response upon the femtosecond laser excitation [22]. It is well known that Bi is a material with a very large SO splitting, and it therefore attracts constant interest in its potential applications in spintronics, where various schemes of combining it with semiconductors are suggested, one of the most recent being an investigation of the BiTeI

*E-mail: khomitsky@phys.unn.ru

bulk material where the SO splitting reaches the very high value 0.4 eV [23].

It is evident from the list of papers mentioned above that the geometric properties of atom arrangement and the resulting band structure have already been studied for Bi/Si systems by many experimental and theoretical groups. But much less attention has been given so far to the prediction and observation of different effects caused by the electron system response to an external excitation, including the basic properties such as the charge current and spin polarization in a dc field, which are often considered the starting point of the response calculations, especially for systems with an important role of SO coupling [24–27]. Besides the response to the dc electric field, the optical properties of an SO-split band spectrum have always attracted significant attention starting from the conventional semiconductor structures with a large SO coupling [28–32]. In our previous papers, we have observed an important role of SO coupling in conventional InGaAs-based semiconductor superlattices in the energy band formation [33], which directly affected both charge and spin response for the excitation by electromagnetic radiation [34, 35] and by a dc electric field [36]. It is known that the spin polarization configurations in semiconductors may have a rather long relaxation time [4, 37, 38], which makes them as important as the conventional charge current setups for applications in nanoelectronics and spintronics.

While there is no doubt that the electron properties in Bi-covered Si interface differ from those in conventional semiconductor structures with strong SO coupling, the questions regarding their SO-dependent response to external dc and electromagnetic fields remain very important because we are still in the beginning of our way toward understanding and utilizing such novel materials with the giant SO coupling as Bi/Si.

The goal of this paper is to apply a modified and expanded version of the simple but adequate nearly free electron model [1] for the band structure of electrons in Bi covering the Si(111) surface, which allows calculating various physical characteristics of this material in the linear response regime, including the charge current and spin polarization caused by a dc electric field with different orientations, and also obtaining the response of nonequilibrium spin polarization excited by an electromagnetic field with various polarizations. Indeed, such physical quantities can be among the first measured in the nearest experiments on Bi/Si, and hence it is interesting to calculate them beforehand both qualitatively and, when possible, quantitatively. Because we do not currently know many material parameters

of the electron system in Bi-covered Si interface exactly, including the parameters such as the electron surface concentration and mobility, the dielectric tensor, the relaxation rates for charge and spin, we sometimes cannot calculate the effects in the absolute measurable units and use the standard label “arbitrary units” instead. Still, we believe that the comparison of the output results for the same physical parameter calculated under different conditions always has a value because it allows predicting their relative significance when the conditions are varied. We find both common and distinct features of the charge and spin system response in Bi/Si compared to the well-known GaAs or InGaAs semiconductor structures. Thus, we believe that our findings can be a good starting point for further theoretical and experimental studies of the charge and spin response in the Bi/Si system in various external fields.

This paper is organized as follows. In Sec. 2, we introduce an expanded version of the nearly free electron Hamiltonian for Bi/Si and discuss the band structure and spin polarization in the energy bands. In Sec. 3, we solve the kinetic equation and calculate the charge current and spin polarization in a dc electric field. In Sec. 4, we study the excited spin polarization in the framework of the linear response theory for different polarizations and frequencies of the incident electromagnetic wave. We give our conclusions in Sec. 5.

2. HAMILTONIAN AND QUANTUM STATES

Several theoretical models for the band structure calculation of Bi/Si electron surface states proposed recently [1] provided a variety of choices for studies of the corresponding Hamiltonian and quantum states. Here, we start with the simplest nearly free electron (NFE) model that was initially proposed for the description of the band structure mainly in the vicinity of the \bar{M} point on the surface Brillouin zone (SBZ) of Bi/Si having a hexagonal shape shown by the dashed contour in Fig. 1. We describe it here only briefly because the detailed derivation and discussion is available in the original paper [1]. The choice of the reciprocal lattice vectors was initially restricted to three vectors \mathbf{G}_1 , \mathbf{G}_2 , and \mathbf{G}_6 connecting four equivalent gamma-points $\bar{\Gamma}^{(0)}$, $\bar{\Gamma}^{(1)}$, $\bar{\Gamma}^{(2)}$, and $\bar{\Gamma}^{(6)}$. In the framework of the NFE approach for each gamma-point, the standard 2×2 Rashba Hamiltonian of a free electron in the $\hat{\sigma}_z$ basis has been written with the origin of the quasimomentum at the corresponding $\bar{\Gamma}^{(n)}$ point. As a result, an 8×8 matrix is derived giving the energy bands and

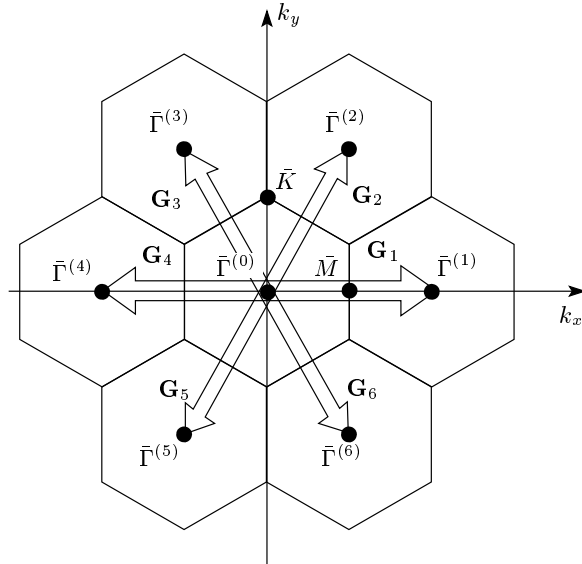


Fig. 1. Surface Brillouin zones of Bi/Si of hexagonal shape shown by solid lines and the reciprocal lattice (hollow) vectors $\mathbf{G}_1, \dots, \mathbf{G}_6$ connecting the equivalent gamma-points $\bar{\Gamma}^{(0)}, \dots, \bar{\Gamma}^{(6)}$ of the nearest-neighbor approximation for the NFE model. The spin-split Rashba parabolics are centered in each of the gamma points

two-component eigenvectors (the Rashba spinors) that describe spin polarization in the reciprocal space.

We use an expanded version of this model by including the remaining reciprocal vectors $\mathbf{G}_4, \mathbf{G}_5$, and \mathbf{G}_3 into our basis of nearest-neighbor sites connecting the central gamma-point $\bar{\Gamma}^{(0)}$ with all surrounding points $\bar{\Gamma}^{(1)}, \dots, \bar{\Gamma}^{(6)}$, as is shown by hollow vectors $\mathbf{G}_1, \dots, \mathbf{G}_6$ in Fig. 1, where several hexagonal SBZs are shown by solid contours, thus creating a 14×14 Hamiltonian matrix. We assume the previously determined [1] values of geometrical parameters $\bar{\Gamma}\bar{M} = 0.54 \text{ \AA}^{-1}$ and $\bar{\Gamma}\bar{K} = 0.62 \text{ \AA}^{-1}$. Such an expansion allows treating a much wider area of the SBZ compared to the region near the \bar{M} point [1] and to keep the symmetry of the nontrivial hexagonal Bi/Si(111) trimer structure with one monolayer of Bi atoms [1, 6, 7, 13].

Our Hamiltonian can thus be described via its matrix elements in the form

$$H_{nn'} = H_R(\mathbf{k} + \mathbf{G}_n)\delta_{nn'} + V_{nn'}, \quad (1)$$

and the electron spinor wavefunction is constructed as

$$\Psi_{\mathbf{k}}(\mathbf{r}) = \sum_n a_{n\mathbf{k}}\psi_{n\mathbf{k}}(\mathbf{r}), \quad (2)$$

where the conventional form of the Rashba Hamiltonian is used,

$$H_R(\mathbf{k}) = \begin{pmatrix} \hbar^2 k^2 / 2m & \alpha_R(k_y + ik_x) \\ \alpha_R(k_y - ik_x) & \hbar^2 k^2 / 2m \end{pmatrix} \quad (3)$$

(α_R is the Rashba parameter), and the matrix elements of the periodic potential coupling the free electron states are

$$V_{nn'} = \langle \psi_n | \sum_m V_0 \exp(i\mathbf{G}_m \cdot \mathbf{r}) | \psi_{n'} \rangle. \quad (4)$$

The basis functions $\psi_{n\mathbf{k}}(\mathbf{r})$ in Eq.(2) are the well-known Rashba spinors $\psi_{n\mathbf{k}} = \psi_{\mathbf{k}+\mathbf{G}_n}$, where

$$\psi_{\mathbf{k}} = \frac{e^{i\mathbf{k}\cdot\mathbf{r}}}{\sqrt{2}} \begin{pmatrix} 1 \\ \pm \exp[i\text{Arg}(k_y - ik_x)] \end{pmatrix}, \quad (5)$$

and the “ \pm ” sign corresponds to two eigenvalues for the Rashba energy spectrum $E(k) = \hbar^2 k^2 / 2m \pm \alpha_R k$. We continue using the known values of material parameters for Eqs. (1)–(4) and constants used in the initial construction [1] of the NFE model for Bi/Si, namely, we put $m = 0.8m_0$, $\alpha_R = 1.1 \text{ eV}\cdot\text{\AA}$, and $V_0 = 0.3 \text{ eV}$.

After diagonalization of Hamiltonian (1), we obtain the energy band spectrum $E = E_s(k_x, k_y)$, where $s = 1, 2, \dots$ labels the energy bands of electrons in the Bi/Si(111) system. A three-dimensional plot of the energy band structure is presented in Fig. 2 for the four lowest bands labeled 1 to 4. These lowest bands seem to be of the primary importance for the electron response analysis because the Fermi level is reportedly located [1] in the middle of them at $E_F = 1.6 \text{ eV}$, i. e., between the band No. 2 and the band No. 3, as can be seen in Fig. 2. One of the most important features of the spectrum in Fig. 2, stemming from the lattice geometry, is the hexagonal symmetry of the energy bands in \mathbf{k} -space, which implies, among other things, the absence of the $k_x \leftrightarrow k_y$ symmetry, leading to rich properties of the spin response phenomena, as we see below. We note that the cross sections of our 3D band plot shown here accurately repeat the 2D plots for the energy dispersion lines along various directions in the SBZ that were studied previously in the framework of the NFE model [1]. We here add just some new quantitative data: the cross sections of the energy band surfaces along the $\bar{\Gamma}$ – \bar{M} direction reported previously [1] may have created an impression of a large energy gap in the whole spectrum between bands 2 and 3, while the complete 3D presentation of these bands in Fig. 2 indicates that the global structure of the energy bands in the whole 2D SBZ leaves this gap open but with

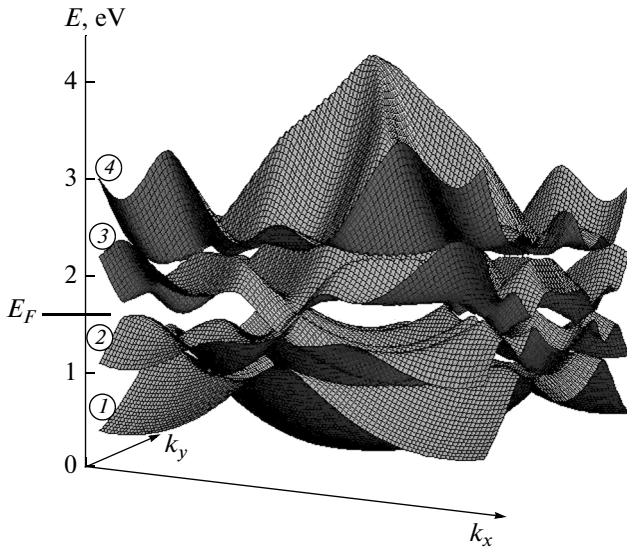


Fig. 2. Energy band structure of electrons on the Bi-covered Si(111) surface for the four lowest bands labeled 1 to 4. The Fermi level is located at $E_F = 1.6$ eV between band No. 2 and band No. 3, where a small global energy gap around 0.1 eV is formed. The cross sections of the 3D band plot shown here accurately repeat the 2D plots for the energy dispersion lines along various directions in the SBZ, which were studied earlier in the framework of the NFE model [1]

a much smaller width around 0.1 eV. Of course, the precise values of energy gaps may vary from model to model and can be specified more precisely in the future experimental and theoretical analysis.

Another important characteristic of quantum states in a system with significant SO coupling is the spin polarization of the eigenstates $\psi_{\mathbf{k}}$ in the Brillouin zone, which can be defined as the vector field in the reciprocal space with the components ($m = x, y, z$)

$$S_m(\mathbf{k}) = \langle \psi_{\mathbf{k}} | \sigma_m | \psi_{\mathbf{k}} \rangle, \quad (6)$$

where σ_m are the Pauli matrices.

As is usual for the Hamiltonian with a pure Rashba SO coupling term, the out-of-plane component S_z of the spin field vanishes. The remaining components form a 2D spin polarization distribution in the SBZ, which creates a specific vector field pattern for each of the energy bands. In Fig. 3 and Fig. 4, we show the 2D spin polarization distributions ($S_x(\mathbf{k}), S_y(\mathbf{k})$) for the lowest energy bands No. 1 (Fig. 3a), No. 2 (Fig. 3b), No. 3 (Fig. 4a), and No. 4 (Fig. 4b) from the band spectrum shown in Fig. 2, with the hexagonal SBZ marked by a solid contour. As for the spins in two lowest subbands shown in Fig. 3, we can see here

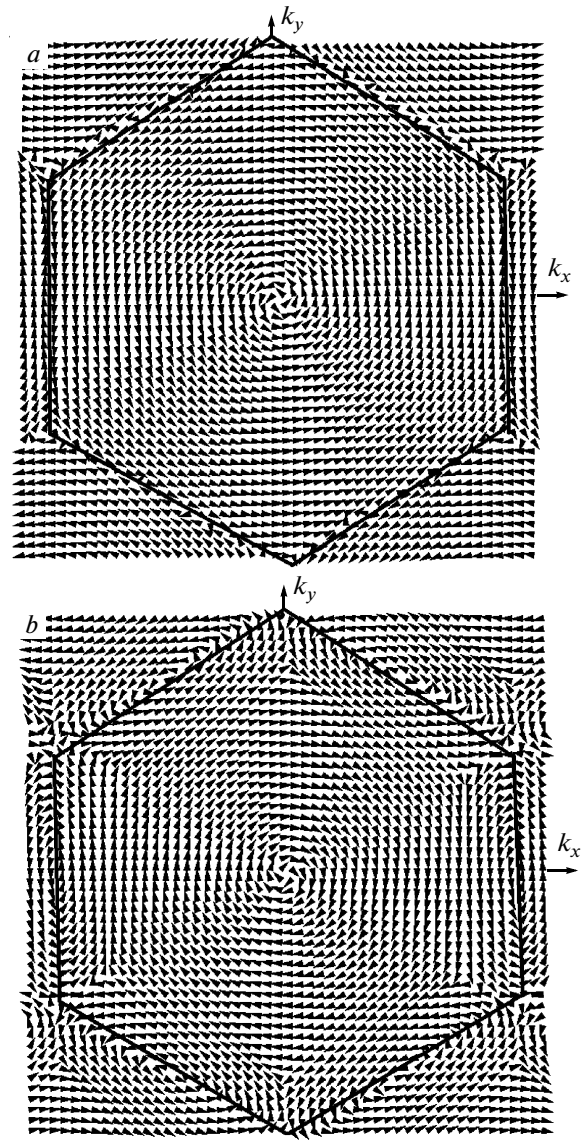


Fig. 3. Spin polarization 2D-distributions ($S_x(\mathbf{k}), S_y(\mathbf{k})$) for the lowest energy bands No. 1 (a) and No. 2 (b) from the band spectrum shown in Fig. 2, with the hexagonal SBZ marked by a solid contour. The initial Rashba counterclockwise and clockwise patterns are present in a wide area surrounding the SBZ center, but a more complicated vector field structure is observed near the SBZ edge

that the initial Rashba counterclockwise and clockwise patterns of spin directions are present in a rather wide area surrounding the SBZ center, but a more complicated vector field structure arises near the SBZ edge. The spin polarization in the higher band No. 3 and especially in band No. 4 shown in Fig. 4 demonstrates new properties compared to the free Rashba states, in-

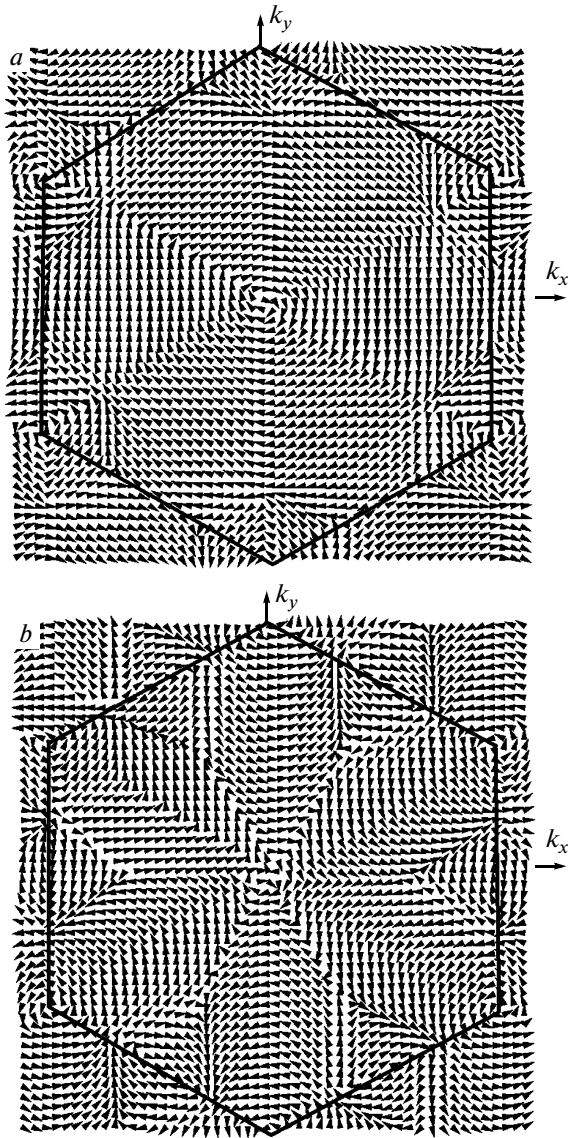


Fig. 4. Spin polarization distributions ($S_x(\mathbf{k}), S_y(\mathbf{k})$) for the higher energy bands No. 3 (a) and No. 4 (b) from the band spectrum shown in Fig. 2, with the hexagonal SBZ marked by a solid contour. The spin polarization in band No. 3 (a) and especially in band No. 4 (b) demonstrates new properties compared to those of the free Rashba states, including both the shape of the spin vector field, which now captures more features of the hexagonal geometry of the SBZ, and the occurrence of new local vortices at various symmetry points of the SBZ, mainly near its corners

cluding both the shape of the spin vector field that now captures more features of the hexagonal geometry of the SBZ, and the emergence of new local vortices at various symmetry points of the SBZ, mainly its corners.

It can be concluded from the analysis of the spin polarization in the energy bands of the Bi/Si system that certain properties of the initial basis of Rashba states remain visible. But the change of the space symmetry to the hexagonal type without an element of the axial symmetry and without the $x \leftrightarrow y$ symmetry may lead to both common and distinct features in the current and spin response to the application of various external fields, compared to the well-known properties of 2D electron gas with the Rashba SO coupling. This assumption is confirmed and illustrated below.

3. CHARGE CURRENT AND SPIN POLARIZATION RESPONSE FOR A DC FIELD

It is known that the response of a 2D electron gas with SO coupling to a constant electric field may be accompanied not only by the charge current but also by spin polarization [26, 27, 36]. The most significant properties of this response for a pure Rashba SO term (3) in the Hamiltonian is the occurrence of the in-plane transverse polarization, i. e., the $S_{y(x)}$ spin component when the electric field is applied along the $x(y)$ direction, while the out-of-plane S_z component is absent in the case of the accurately included relaxation processes, which is sometimes also related to the absence of the spin Hall effect for a \mathbf{k} -linear Rashba model in the presence of disorder [39]. It is therefore natural to start the analysis of the electron system response with the calculation of the charge current and field-induced spin.

We start with the calculation of the nonequilibrium electric-field-induced distribution function $\tilde{f}_m(\mathbf{k}, E_i)$ in the m th energy band. If the system is subjected to a constant and uniform electric field E_i parallel to the i th axis, then the kinetic equation for $\tilde{f}_m(\mathbf{k}, E_i)$ can be written in the collision frequency approximation as [36]

$$eE_i \frac{\partial \tilde{f}_m(\mathbf{k}, E_i)}{\partial k_i} = -\nu [\tilde{f}_m(\mathbf{k}, E_i) - f_m(\mathbf{k})], \quad (7)$$

where ν is the collision rate and

$$f_m(\mathbf{k}) = \left\{ 1 + \exp \left[\frac{E_m(\mathbf{k}) - \mu}{k_B T} \right] \right\}^{-1}$$

is the Fermi equilibrium distribution function in the m th band. Because the Bi/Si energy spectrum is characterized by a very large SO splitting and the band widths of the order of 1 eV, it may be a promising candidate for spin-dependent phenomena visible at room temperature. In what follows, we assume that

$T = 293$ K and consider the value $\nu = 10^{12} \text{ s}^{-1}$. As we have noted, the estimate for the collision rate as well as for many other material parameters for the Bi/Si system is presently based on the assumptions rather than on solid experimental facts because we are still in the beginning of the investigation of this new material. Still, we believe that our qualitative and sometimes quantitative results can be useful for predicting some novel properties of the electron and spin system response.

The mean charge current density $j_i(E_i)$ measured for a 2D system in the units of current divided by the units of transverse system size and the mean spin polarization S_j , $j = x, y, z$, can be found as [36]

$$j_i(E_i) = en \sum_{m, \mathbf{k}} \langle \psi_{m\mathbf{k}} | v_i | \psi_{m\mathbf{k}} \rangle \tilde{f}_m(\mathbf{k}, E_i), \quad (8)$$

$$S_j(E_i) = \sum_{m, \mathbf{k}} \langle \psi_{m\mathbf{k}} | \sigma_j | \psi_{m\mathbf{k}} \rangle \tilde{f}_m(\mathbf{k}, E_i), \quad (9)$$

where n is the surface concentration of electrons on the Bi-covered Si surface, and the velocity operator $v_i = \partial H / \partial k_i$ includes the SO part proportional to the Rashba parameter α_R and acts on spinor wavefunctions (2) via the matrices

$$v_x = \begin{pmatrix} -i\hbar\nabla_x/m & i\alpha_R/\hbar \\ -i\alpha_R/\hbar & -i\hbar\nabla_x/m \end{pmatrix}, \quad (10)$$

$$v_y = \begin{pmatrix} -i\hbar\nabla_y/m & \alpha_R/\hbar \\ \alpha_R/\hbar & -i\hbar\nabla_y/m \end{pmatrix}. \quad (11)$$

To take a closer look on the expectations of the charge current density, we calculate $j_x(E_x)$ and $j_y(E_y)$ as well as $S_i(E_x)$ and $S_i(E_y)$ ($i = x, y, z$) by applying Eq. (8) for the electron surface concentration $n = 10^{14} \text{ cm}^{-2}$, which may be reasonable because the surface density of atoms on the Bi-covered Si(111) surface is estimated to be of the order of 10^{15} cm^{-2} according to experimental observations [9, 10].

The results for charge current density (8) and spin polarization (9) are shown in Fig. 5. We can see a conventional linear dependence of the charge current on the applied electric field throughout the whole range of fields up to 2 kV/cm, and an almost linear dependence for the significant nonzero induced spin components $S_y(E_x)$ and $S_x(E_y)$. The other in-plane components $S_x(E_x)$ and $S_y(E_y)$ are also present in Fig. 5, but their magnitude is much lower compared to $S_y(E_x)$ and $S_x(E_y)$, and the out-of-plane S_z component is negligibly small. It is evident that the lattice asymmetry with

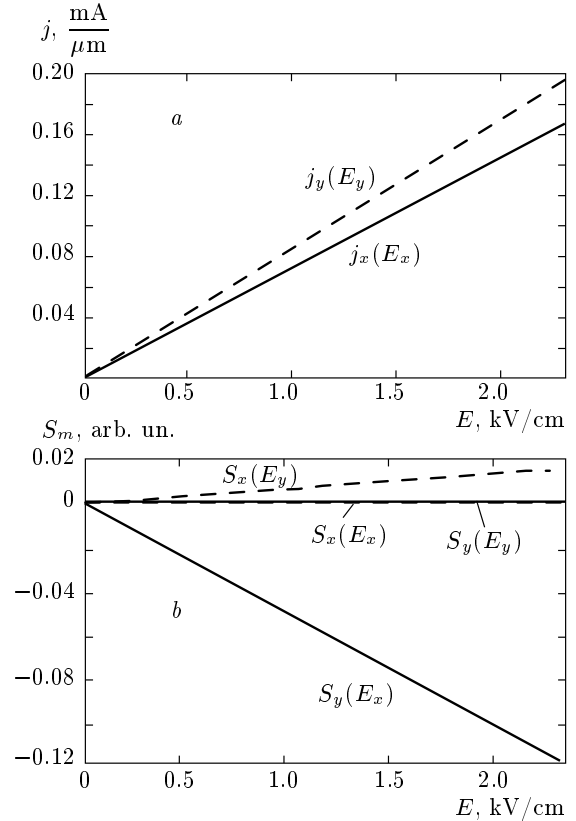


Fig. 5. (a) Charge current density (8) and (b) spin polarization (9) induced by a dc electric field applied along x (solid curves) and y (dashed curves). The conventional linear dependence of the charge current on the applied electric field in the whole range of fields and an almost linear dependence for the significant nonzero induced spin components $S_y(E_x)$ and $S_x(E_y)$ are visible. The other in-plane components, $S_x(E_x)$ and $S_y(E_y)$, are also present but their magnitude is much lower, and the out-of-plane S_z component is negligibly small

respect to the $x \leftrightarrow y$ interchange leads to a slight but distinct asymmetry in the current amplitude around 12 %, and the dominant $S_y(E_x)$ and $S_x(E_y)$ induced spin components demonstrate the well-known transverse in-plane character of the induced spin for the linear Rashba SO coupling. We note that the local probe measurements of induced spin polarizations (or magnetization) may detect a nonzero static and dynamic local magnetization [40] in the spot under the probe even in the case of total zero mean spin value (9). The examples of such systems with the zero total spin polarization but a nonzero spin spatial distribution (spin textures) can be found among the models of semiconductor superlattices with SO coupling both with [35] and without [34, 36] an external magnetic field, but their experi-

mental observation and device application are currently limited by the probe and manipulation technology of the size of artificial superlattices and quantum wells rather than probing and utilizing the spatial magnetic configurations on the scale of individual atoms in the lattice. As regards the predicted nonzero mean values of the induced spin, such as those predicted here for Bi/Si, they are related to the whole sample and should therefore be detectable. We believe that the predictions of the charge current and spin polarization generation made in this section can be useful in designing novel spintronic devices where the induced spin components are coupled in a well-defined manner to the direction of the applied electric field, and this effect survives at room temperature and finite collision rate.

4. SPIN POLARIZATION EXCITED BY AN ELECTROMAGNETIC FIELD

The response of the spin system in materials with significant SO coupling to the application of an external electromagnetic radiation is among the most important and straightforwardly obtained characteristics because the optical manipulation of spins is one of the main goals of spintronics in general, and the linear response theory for the electromagnetic radiation effects is well established and easily applied. It was found in various papers that the spins with different polarizations can be excited, depending on the symmetry of the electron Hamiltonian, the type and strength of the SO terms, and the polarization of incident radiation [2, 3, 28–31, 34, 35]. As in the preceding section, we calculate the response functions for the room temperature and for a realistic collision broadening, because the relatively large scale of energy bands and SO splitting in the Bi/Si electron system compared to the conventional GaAs, InGaAs, or pure Si semiconductor structures can make Bi/Si a promising candidate for the observation and control of the predicted radiation-induced effects in the devices operating even at room temperatures, as we hope.

The electromagnetic wave is considered to be propagating normally to the Bi/Si(111) interface along the z axis, and is characterized by the polarization of the electric field vector $\mathbf{E} = \mathbf{E}_0 \exp[i(\mathbf{k} \cdot \mathbf{r} - \omega t)]$ in the xy plane, $\mathbf{E}_0 = (E_{0x}, E_{0y}, 0)$. In the dipole approximation, the interaction of the electromagnetic field with the electrons is described by velocity operators (10) and (11), which include the SO part. We start with the calculation of the absorption coefficient

$$\alpha(\omega) = \frac{4\pi^2 e^2}{m^2 \omega c \sqrt{\varepsilon} V} \sum_{n, n', \mathbf{k}} |(\mathbf{e} \cdot \mathbf{v})_{nn'\mathbf{k}}|^2 \times \delta(E_{n'\mathbf{k}} - E_{n\mathbf{k}} - \hbar\omega) (f_{n\mathbf{k}} - f_{n'\mathbf{k}}), \quad (12)$$

where $\mathbf{e} = (e_x, e_y, 0)$ is the polarization vector for the incident wave, $\mathbf{v} = (v_x, v_y, 0)$ is given by velocity operators (10) and (11), $f_{n\mathbf{k}}$ and $f_{n'\mathbf{k}}$ are Fermi equilibrium distribution functions, V is the sample volume, and the summation is taken over all energy bands n, n' and the SBZ points \mathbf{k} . As we have already noted, we do not yet know the exact values of many material parameters for Bi/Si, including the dielectric constant ε , and we therefore focus mainly on the dependence of (12) on the incident wave frequency and scale the absolute value of absorption in arbitrary units, which can always be rescaled when the values of material parameters are clarified in future experiments.

The second quantity whose frequency dependence we present together with the absorption is the induced spin polarization $S_m(\omega)$, which can be derived by applying the Kubo linear response theory [35, 41, 42] and has the form

$$S_m(\omega) = -\frac{ieE_{0l}}{8\pi m\hbar} \sum_{n, n', \mathbf{k}} \frac{f_{n\mathbf{k}} - f_{n'\mathbf{k}}}{\omega_{nn'}(\mathbf{k})} \times \frac{S_{n'n}^{(m)}(\mathbf{k}) v_{nn'}^{(l)}(\mathbf{k})}{\omega - \omega_{nn'}(\mathbf{k}) + i\nu}. \quad (13)$$

Here, the interband matrix elements of the spin m th component operator $S_{n'n}^{(m)}(\mathbf{k}) = \langle \psi_{n'\mathbf{k}} | \hat{\sigma}_m | \psi_{n\mathbf{k}} \rangle$ as well as the matrix elements for the l th component of velocity operators (10) and (11) enter depending on the incident wave polarization $l = x, y$ and on the desirable output for the spin component, $\hbar\omega_{nn'}(\mathbf{k}) = E_{n\mathbf{k}} - E_{n'\mathbf{k}}$, the parameter ν is the level broadening, which we take to be equal to the collision rate introduced in the preceding section. As before, we assume that $T = 293$ K and $\nu = 10^{12} \text{ s}^{-1}$, which should provide us with realistic estimates for the absorption and the induced spin dependence on the incoming photon energy.

The results for the photon energy dependence of absorption coefficient (12) and induced spin polarization (13) are shown in Figs. 6–9 for the incident wave linearly polarized along x (Fig. 6) and y (Fig. 7) directions, and for circular σ^+ (Fig. 8) and σ^- (Fig. 9) polarizations. The photon energy interval is chosen to cover the whole energy band range of the four lowest bands shown in Fig. 2, where the most effective transitions occur between the states below and above the Fermi level. We can see that both the in-plane spin components S_x and S_y and the out-of-plane component S_z can be excited on a comparable scale, which is a

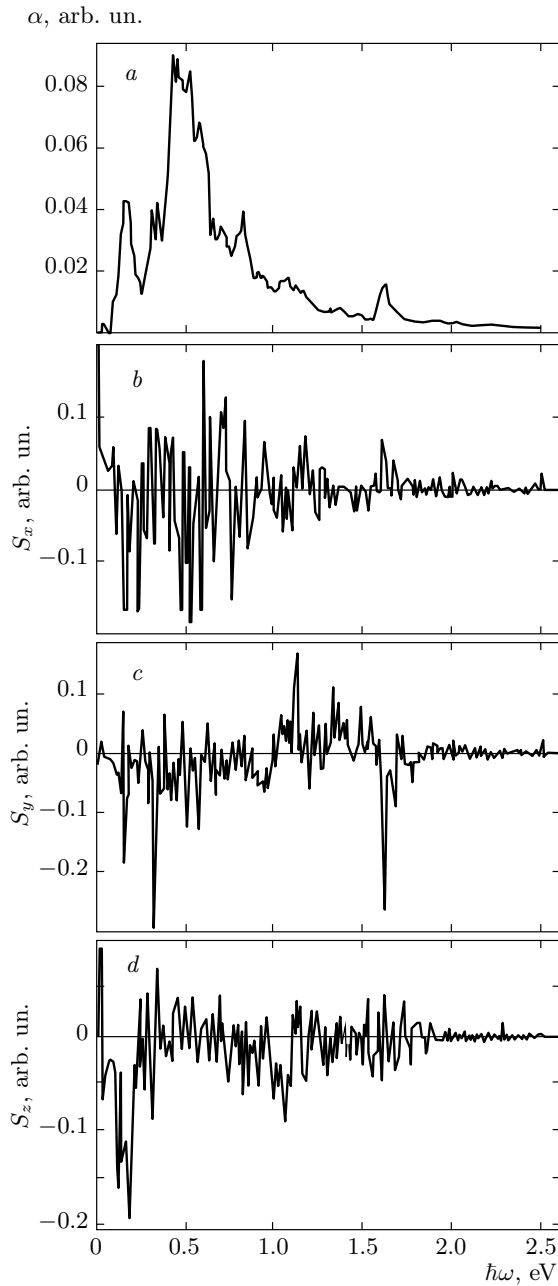


Fig. 6. (a) Absorption coefficient and (b)–(d) components of the induced spin density in the Bi/Si surface electron gas shown as a function of the incoming photon energy for the linear x -polarized incident radiation propagating normally to the interface plane. The greatest absorption and most of the spin polarization peaks are induced at the photon energy $\hbar\omega \approx 0.5$ eV corresponding to the transitions between the highest occupied band 2 and the lowest unoccupied band 3 of the electron energy spectrum shown in Fig. 2. Both the in-plane spin components S_x and S_y and the out-of-plane component S_z can be excited

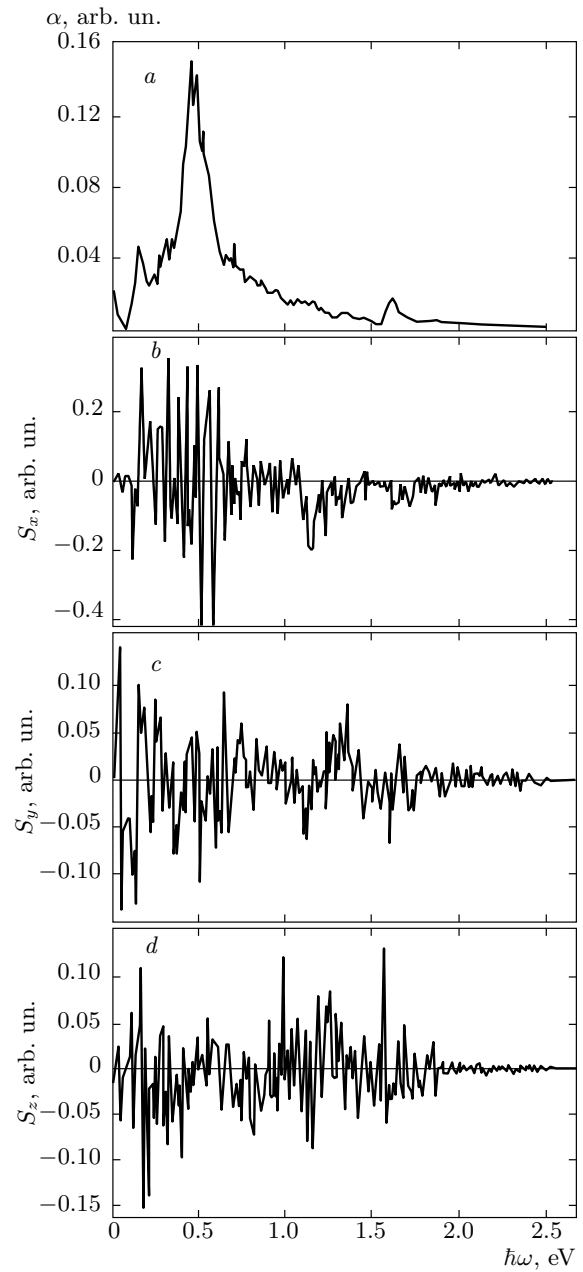


Fig. 7. The same as in Fig. 6 but for y -polarized incident radiation. The $x \leftrightarrow y$ lattice and energy band asymmetry in the hexagonal geometry is reflected in the different shapes and amplitude for the absorption coefficients in this figure and in Fig. 6. The Rashba term in the SO coupling is reflected in the dominant excited S_x component in this figure and the dominating S_y component in Fig. 6

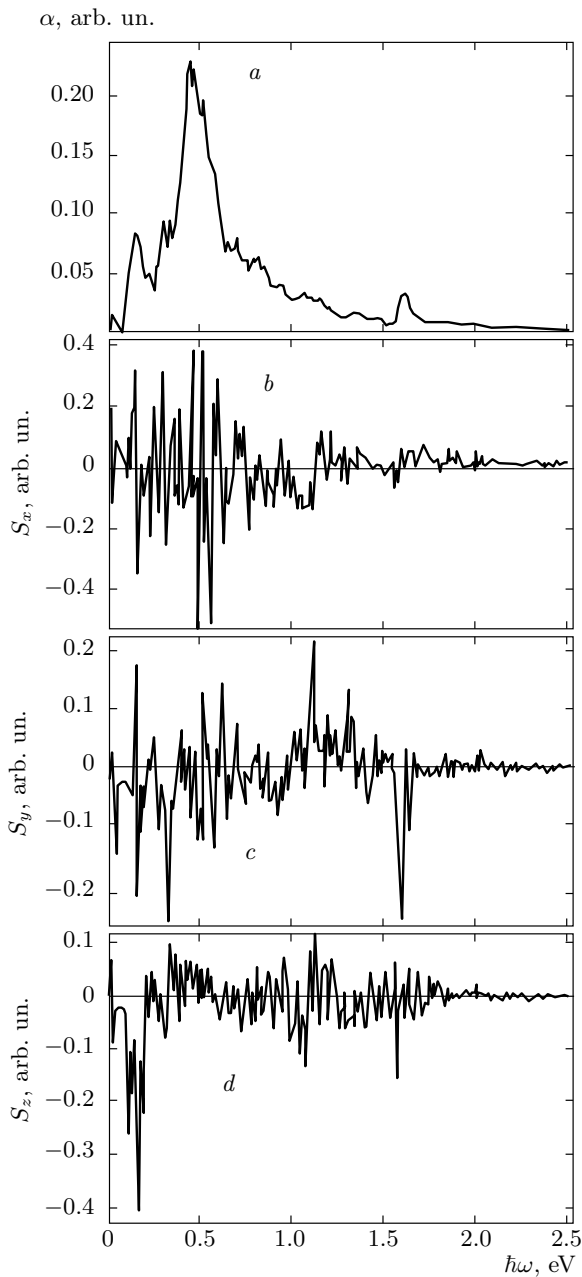


Fig. 8. The same as in Fig. 6 but for circular σ^+ -polarized incident radiation. The common features of the response to both x -polarized and y -polarized incoming waves in Fig. 6 and Fig. 7 can be seen on the spin component figures

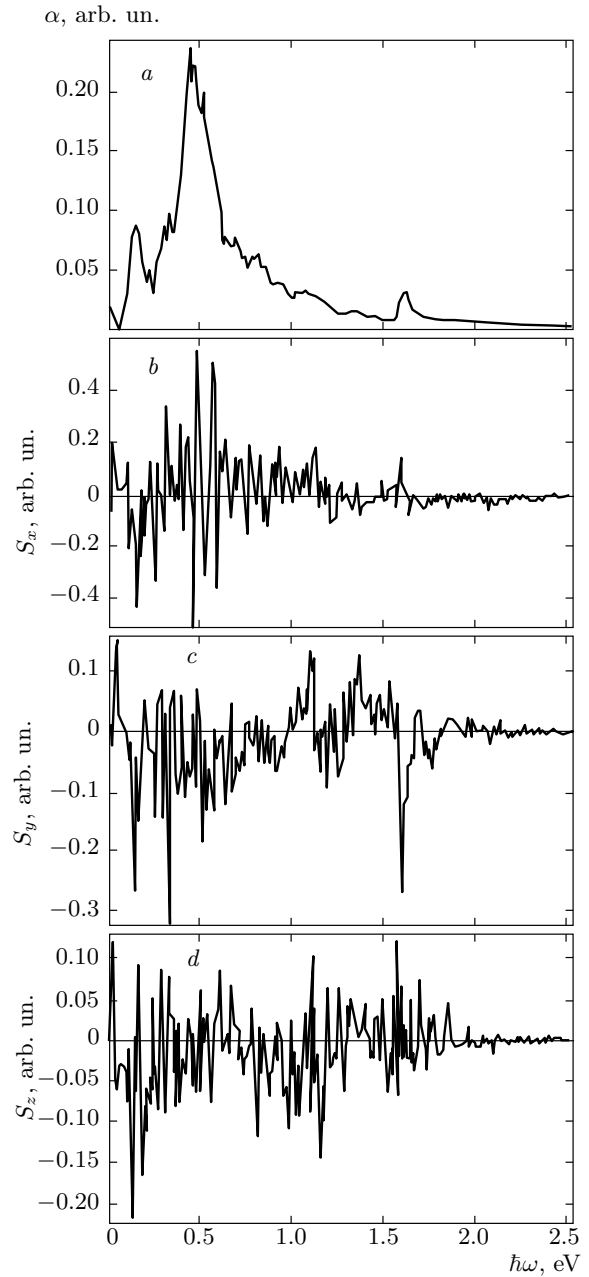


Fig. 9. The same as in Fig. 6 but for circular σ^- -polarized incident radiation. The absorption coefficient is unchanged compared with the σ^+ case in Fig. 8a, but the excited spin components demonstrate quantitative differences while maintaining the same type of shape for the photon energy dependence

distinguishable feature of the lower hexagonal symmetry combined with the Rashba SO coupling compared with one-dimensional [26, 34, 36] or two-dimensional square [35] lattices with the Rashba SO coupling.

If we compare the results for x - and y -polarized ra-

diation in Fig. 6 and Fig. 7, we see that similarly to the dc current properties discussed in the preceding section, the $x \leftrightarrow y$ lattice and energy band asymmetry in the hexagonal geometry of the whole problem is reflected here in the different shapes and amplitudes for

the absorption coefficients in Figs. 6a and 7a. Again, by looking at the relative magnitude of the excited spin components in Figs. 6b–6d and in Figs. 7b–7d, we can see that the pure Rashba SO coupling is reflected in the dominant excited S_x component in Fig. 6 and correspondingly in the dominant S_y component in Fig. 6, i. e., in the in-plane and transverse directions relative to the electric field vector of the incident wave. As regards the results for the circular σ^\pm -polarized radiation presented in Fig. 8 and Fig. 9, the common features of the response to both the x -polarized and y -polarized incoming wave in Fig. 6 and Fig. 7 can be seen on the spin component figures because both v_x and v_y operators here enter expressions (12) and (13) for the response. The absorption coefficient is totally insensitive to the direction of rotation for the incoming wave, as can be seen by comparing Fig. 8a and Fig. 9a. The shape of the photon energy dependence for the excited spin components in Fig. 8b–d and Fig. 9b–d is different for the σ^+ and σ^- polarizations, but these differences have a quantitative rather than a qualitative character because the hexagonal symmetry of the lattice and the energy bands does not make any of these two polarizations preferable from the standpoint of the response quantities in (12) and (13).

In conclusion, the calculation and analysis of the absorption and spin polarization response to monochromatic electromagnetic radiation with normal incidence and different polarizations demonstrate that this radiation is most effectively absorbed in the photon energy range around 0.5 eV corresponding to the photon wavelength $\lambda = 2.47\mu\text{m}$, where both in-plane and out-of-plane spin components can be excited at realistic temperature and collision broadening on a comparable scale with the relative amplitudes depending on the precise value of the frequency and polarization of the incident radiation. These properties can be useful for designing new optical and spintronic devices coupling the electron spin with light and operating at room temperature.

5. CONCLUSIONS

We have extended the nearly free-electron model [1] describing the energy bands and spin polarization for electron states at the Bi/Si(111) interface with the giant spin–orbit coupling, and applied it for the linear response analysis of the charge current and induced spin caused by a dc field and by electromagnetic radiation. It was found that the large spin–orbit coupling in this system may allow resolving the spin-dependent

properties even at room temperature and at a realistic collision rate. The geometry of the atomic lattice combined with spin–orbit coupling leads to an anisotropic response for both the current and the spin components related to the orientation of the external field. The in-plane dc electric field produces only the in-plane components of spin in the sample, while both in-plane and out-of-plane spin components can be excited by normally propagating electromagnetic waves with different polarizations. The qualitative predictions of the charge and spin response in a novel and promising Bi/Si system may be useful for the forthcoming detailed theoretical and experimental studies, which may lead to the development of principally new electronic, optical, and spintronic devices operating at room temperature. Further theoretical and especially experimental studies of this promising system with a large SO coupling allowing the spin-related effects to survive at room temperature are expected to lead to new and fascinating phenomena with both fundamental, experimental, and device-related results.

The author is grateful to V. Ya. Demikhovskii, A. M. Satanin, and A. A. Perov for helpful discussions and to A. A. Chubanov for technical assistance. The work was supported by the RFBR (Grants Nos. 11-02-00960a and 11-02-97039/Regional) and by the RNP Program of the RF Ministry of Education and Science.

REFERENCES

1. E. Frantzeskakis, S. Pons, and M. Grioni, *Phys. Rev. B* **82**, 085440 (2010).
2. *Semiconductor Spintronics and Quantum Computation*, ed. by D. D. Awschalom, D. Loss, and N. Samarth, Springer, Berlin (2002).
3. I. Žutić, J. Fabian, and S. Das Sarma, *Rev. Mod. Phys.* **76**, 323 (2004).
4. M. W. Wu, J. H. Jiang, and M. Q. Weng, *Phys. Rep.* **493**, 61 (2010).
5. R. Shioda, A. Kawazu, A. A. Baski et al., *Phys. Rev. B* **48**, 4895 (1993).
6. R. H. Miwa and G. P. Srivastava, *Phys. Rev. B* **66**, 235317 (2002).
7. R. H. Miwa, T. M. Schmidt, and G. P. Srivastava, *J. Phys. C* **15**, 2441 (2003).
8. T. Hirahara, T. Nagao, I. Matsuda et al., *Phys. Rev. Lett.* **97**, 146803 (2006).

9. T. Hirahara, T. Nagao, I. Matsuda et al., *Phys. Rev. B* **75**, 035422 (2007).
10. T. Hirahara, K. Miyamoto, I. Matsuda et al., *Phys. Rev. B* **76**, 153305 (2007).
11. E. Frantzeskakis, S. Pons, H. Mirhosseini et al., *Phys. Rev. Lett.* **101**, 196805 (2008).
12. J. H. Dil, F. Meier, J. Lobo-Checa et al., *Phys. Rev. Lett.* **101**, 266802 (2008).
13. I. Gierz, T. Suzuki, E. Frantzeskakis et al., *Phys. Rev. Lett.* **103**, 046803 (2009).
14. G. Bian, T. Miller, and T.-C. Chiang, *Phys. Rev. B* **80**, 245407 (2009).
15. K. Sakamoto, H. Kakuta, K. Sugawara et al., *Phys. Rev. Lett.* **103**, 156801 (2009).
16. G. Jnawali, H. Hattab, B. Krenzer, and M. Horn von Hoegen, *Phys. Rev. B* **74**, 195340 (2006).
17. G. Jnawali, H. Hattab, F. J. Meyer zu Heringdorf et al., *Phys. Rev. B* **76**, 035337 (2007).
18. R. H. Miwa, T. M. Schmidt, and P. Venezuela, *Phys. Rev. B* **72**, 125403 (2005).
19. J. Mysliveček, F. Dvořák, A. Stróžecka, and B. Voigtländer, *Phys. Rev. B* **81**, 245427 (2010).
20. R. H. Miwa and G. P. Srivastava, *Phys. Rev. B* **74**, 035301 (2006).
21. R. H. Miwa, W. Orellana, and G. P. Srivastava, *Phys. Rev. B* **78**, 115310 (2008).
22. A. Hanisch, B. Krenzer, T. Pelka et al., *Phys. Rev. B* **77**, 125410 (2008).
23. M. S. Bahramy, R. Arita, and N. Nagaosa, arXiv:1105.2757.
24. V. M. Edelstein, *Sol. St. Comm.* **73**, 233 (1990).
25. A. G. Aronov, Yu. B. Lyanda-Geller, and G. E. Pikus, *Zh. Eksp. Teor. Fiz.* **100**, 973 (1991).
26. P. Kleinert, V. V. Bryksin, and O. Bleibaum, *Phys. Rev. B* **72**, 195311 (2005).
27. O. E. Raichev, *Phys. Rev. B* **75**, 205340 (2007).
28. R. D. R. Bhat, F. Nastos, Ali Najmaie, and J. E. Sipe, *Phys. Rev. Lett.* **94**, 096603 (2005).
29. A. Najmaie, E. Ya. Sherman, and J. E. Sipe, *Phys. Rev. Lett.* **95**, 056601 (2005).
30. S. A. Tarasenko, *Phys. Rev. B* **72**, 113302 (2005).
31. S. Giglberger, L. E. Golub, V. V. Bel'kov et al., *Phys. Rev. B* **75**, 035327 (2007).
32. Z.-G. Zhu, C.-L. Jia, and J. Berakdar, *Phys. Rev. B* **82**, 235304 (2010).
33. V. Ya. Demikhovskii and D. V. Khomitsky, *Pis'ma v Zh. Eksp. Teor. Fiz.* **83**, 399 (2006).
34. D. V. Khomitsky, *Phys. Rev. B* **77**, 113313 (2008).
35. A. A. Perov, L. V. Solnyshkova, and D. V. Khomitsky, *Phys. Rev. B* **82**, 165328 (2010).
36. D. V. Khomitsky, *Phys. Rev. B* **79**, 205401 (2009).
37. Y. V. Pershin, *Phys. Rev. B* **71**, 155317 (2005).
38. P. Stano and J. Fabian, *Phys. Rev. B* **74**, 045320 (2006).
39. J. I. Inoue, G. E. W. Bauer, and L. W. Molenkamp, *Phys. Rev. B* **70**, 041303(R) (2004).
40. A. Neudert, J. McCord, D. Chumakov et al., *Phys. Rev. B* **71**, 134405 (2005).
41. R. Kubo, *J. Phys. Soc. Jpn.* **12**, 570 (1957).
42. C. S. Wang and J. Callaway, *Phys. Rev. B* **9**, 4897 (1974).